Many-electron effects on x-ray Rayleigh scattering by highly charged He-like ions

A. V. Volotka,[1,2] V. A. Yerokhin,[3] A. Surzhykov,[1] Th. Stöhlker,[1,4,5] and S. Fritzsche[1,5]
[1]*Helmholtz-Institut Jena, D-07743 Jena, Germany*
[2]*Department of Physics, St. Petersburg State University, 198504 St. Petersburg, Russia*
[3]*Center for Advanced Studies, Peter the Great St. Petersburg Polytechnic University, 195251 St. Petersburg, Russia*
[4]*GSI Helmholtzzentrum für Schwerionenforschung, D-64291 Darmstadt, Germany*
[5]*Theoretisch-Physikalisches Institut, Friedrich-Schiller-Universität Jena, D-07743 Jena, Germany*
(Received 11 December 2015; published 16 February 2016)

The Rayleigh scattering of x rays by many-electron highly charged ions is studied theoretically. The many-electron perturbation theory, based on a rigorous quantum electrodynamics approach, is developed and implemented for the case of the elastic scattering of (high-energetic) photons by heliumlike ions. Using this elaborate approach, we here investigate the many-electron effects beyond the independent-particle approximation (IPA) as conventionally employed for describing the Rayleigh scattering. The total and angle-differential cross sections are evaluated for the x-ray scattering by heliumlike Ni^{26+}, Xe^{52+}, and Au^{77+} ions in their ground state. The obtained results show that, for high-energetic photons, the effects beyond the IPA do not exceed 2% for the scattering by a closed K shell.

DOI: 10.1103/PhysRevA.93.023418

I. INTRODUCTION

The elastic scattering of a light by bound electrons is commonly known as Rayleigh scattering. It has been found to be a powerful and versatile tool for investigating the structure and dynamics of bound electrons as well as for probing the atomic environment. Apart from the fundamental interest, a quantitative understanding of the Rayleigh scattering is needed in various fields, including the study of the solid-state, complex molecules or even nano-objects [1–4], astrophysics [5,6], as well as in medical diagnostics [7].

Experimentally, recent progress in exploring the Rayleigh scattering of hard x rays by atomic or solid-state targets has been achieved by a major improvement of the detection techniques as well as the quality of light sources. Indeed, novel solid-state photon detectors [8,9] together with advances in the available synchrotron sources [10] have paved the way towards new generations of experiments. For example, a measurement of the linear polarization of the Rayleigh scattered light has been recently performed with the help of the segmented solid-state detectors at the PETRA III synchrotron at DESY [11]. The advances in the Rayleigh scattering experiments nowadays also demand further and accurate predictions at the side of theory.

The theoretical investigations on the elastic scattering of photon by bound electrons dates back to the mid-1930s [12]. While initially quite simple approximations were applied, based on the atomic form factors, the rigorous quantum electrodynamical (QED) approach has later been developed by using the relativistic second-order S-matrix amplitude; we refer the reader to Ref. [13] for a comprehensive historical overview. This latter approach has now become the standard for treating the Rayleigh scattering. These developments were triggered specially by the pioneering work of Brown, Peierls, and Woodward [14], who developed the method for the calculation of the second-order transition amplitudes. Within this QED approach, quite a number of calculations were carried out for different atoms and photon energies [15–21]; we refer the reader to Ref. [22] for a comprehensive review on this approach. In recent years [23–27] the angular and polarization correlation between the incident and outgoing photons have also been investigated. Unfortunately, however, the formalism of the second-order S-matrix theory does not enable one to investigate systematically the many-electron effects on the Rayleigh scattering. This is caused by the electron-electron interaction that is treated only approximately in this formalism by means of a central screening potential, and which is known as screening potential or independent-particle approximation (IPA). Until the present, many-electron effects beyond the IPA were only investigated for the helium atom in Ref. [28]. It was found that the interelectronic-interaction corrections beyond the IPA significantly modify the Rayleigh cross section for the low-energy photons and disappear for higher energies. The main aim of the present study is to investigate the many-electron effects for highly charged ions.

In this paper, we present a rigorous QED treatment of the Rayleigh scattering of light by highly charged heliumlike ions. The QED perturbation expansion with regard to the interelectronic interaction is applied up to the first order for the Rayleigh scattering as an important light-matter interaction process at medium and high photon energies. In particular, formulas have been derived for the zeroth- and first-order interelectronic-interaction corrections to the scattering amplitude. This framework enables one to systematically investigate the many-electron effects beyond the IPA. In Sec. II, the details of this formalism are presented, while the computational techniques and methods are discussed in Sec. III. The total and angle-differential cross sections are evaluated for the scattering of x rays on the ground state of heliumlike Ni^{26+}, Xe^{52+}, and Au^{77+} ions. We shall here consider especially two experimental scenarios in which the incoming light is either unpolarized or completely linearly polarized. In Sec. IV, the obtained numerical results are presented and discussed. Attention is paid to the comparison between the IPA and the many-electron description. For the Rayleigh scattering of x rays by heliumlike ions in their ground state, we find that the many-electron effects beyond the IPA treatment do not exceed

2%. In Sec. V, we briefly summarize our results and give a brief outlook.

Relativistic units ($\hbar = 1, c = 1, m = 1$) and the Heaviside charge unit [$\alpha = e^2/(4\pi)$, $e < 0$] are used throughout the paper.

II. THEORETICAL BACKGROUND

The process of elastic photon scattering is characterized by the energy conservation of the incident and outgoing photons in the center-of-mass frame of the overall scattering system. This means that no energy transfer is possible between the photon and the target with its internal degree of freedom. However, since the energy of the scattered photon is typically much smaller than the atom's rest-mass energy, we therefore consider in the following the scattering of a photon in the rest frame of the atom, so that the incoming and outgoing photon energies simply remain the same. For the theoretical description of (quite) heavy atoms, moreover, it is naturally to utilize the Furry picture, in which the (infinitely heavy) nucleus is taken as the source of the classical Coulomb field and where the interaction of electrons with this field is then treated exactly by just solving the Dirac equation in the nuclear Coulomb potential.

According to the basic principles of QED [29], the differential cross section for the scattering of a photon by an atom is given by

$$d\sigma(k_f,\boldsymbol{\epsilon}_f,A';k_i,\boldsymbol{\epsilon}_i,A) = (2\pi)^4 |\tau_{\gamma_f,A';\gamma_i,A}|^2 \delta\big(E_{A'} + k_f^0 - E_A - k_i^0\big)\, d\mathbf{k}_f, \quad (1)$$

where the initial and final state of the photon are characterized by the four-momentum k_i^μ and k_f^μ and polarization vectors $\boldsymbol{\epsilon}_i$ and $\boldsymbol{\epsilon}_f$, respectively. Here, the zero and spatial components of the four-vector define the photon frequency $k^0 \equiv \omega$ and the photon wave vector $\mathbf{k}$. Moreover, the total energy of the bound electrons are E_A and $E_{A'}$ for the initial and final state of the atom. The shorthand notations A and A' stand for a unique specification of the bound-electron states $A = \alpha_A J_A M_A$ and $A' = \alpha_{A'} J_{A'} M_{A'}$, where J_A and $J_{A'}$ are the total angular momenta, M_A and $M_{A'}$ their corresponding projections, and where α_A and $\alpha_{A'}$ denote all additional quantum numbers that are needed for a unique specification of the states. The energy conservation $E_A = E_{A'}$ clearly shows that no energy transfer occurs to the atom and that the moduli of the wave vectors are the same for the incoming and outgoing photons, $k_i^0 = k_f^0$. Thus, the angle-differential cross section for the elastic scattering in a solid angle $d\Omega_f$ takes the form,

$$d\sigma(\mathbf{k}_f;\mathbf{k}_i,\boldsymbol{\epsilon}_i) = \frac{(2\pi)^4 \big(k_i^0\big)^2}{2J_A+1} \sum_{M_A,\,M_{A'}} \sum_{\boldsymbol{\epsilon}_f} |\tau_{\gamma_f,A';\gamma_i,A}|^2\, d\Omega_f. \quad (2)$$

The scattering amplitude $\tau_{\gamma_f,A';\gamma_i,A}$ can be related to the scattering S-matrix element by the following expression:

$$S^{\rm scat}_{\gamma_f,A';\gamma_i,A} = \langle k_f,\boldsymbol{\epsilon}_f,A'|(\hat{S}-\hat{I})|k_i,\boldsymbol{\epsilon}_i,A\rangle = 2\pi i\ \tau_{\gamma_f,A';\gamma_i,A}\,\delta\big(k_f^0 - k_i^0\big), \quad (3)$$

and where $\hat{S}$ and $\hat{I}$ denote the scattering and identity operators. The scattering S-matrix element $S^{\rm scat}_{\gamma_f,A';\gamma_i,A}$ contains two types of processes: the scattering by the Coulomb potential of the nucleus as well as the scattering by the bound electrons. The first type corresponds to the Delbrück scattering amplitude, while the second one is usually defined as the Rayleigh scattering by the bound electrons. Here, we restrict ourselves to the Rayleigh scattering only. In order to evaluate the corresponding Rayleigh S-matrix element, which we denote as $S^{\rm R}_{\gamma_f,A';\gamma_i,A}$, one has to employ the bound-electron QED perturbation theory. For this purpose, we here utilize the (so-called) two-time Green-function method as developed in Refs. [30–32], where the perturbation theory is formulated for the two-time Green functions. The Rayleigh S-matrix element can be generally related to the two-time Green functions by the equation [32],

$$\begin{aligned} S^{\rm R}_{\gamma_f,A';\gamma_i,A} &= Z_3^{-1}\,\delta\big(k_f^0 - k_i^0\big) \oint_{\Gamma_A} dE' \oint_{\Gamma_A} dE\, g_{\gamma_f,A';\gamma_i,A}\big(E',E,k_i^0\big) \\ &\quad\times \left[\frac{1}{2\pi i}\oint_{\Gamma_A} dE\, g_{A'A'}(E)\right]^{-1/2} \\ &\quad\times \left[\frac{1}{2\pi i}\oint_{\Gamma_A} dE\, g_{AA}(E)\right]^{-1/2}, \end{aligned} \quad (4)$$

where the contour Γ_A encloses the pole corresponding to the bound-electron states with the energy E_A. This contour also excludes all further singularities of the Green functions $g_{\gamma_f,A';\gamma_i,A}$, g_{AA}, and $g_{A'A'}$, which are defined in a similar way as in Ref. [32]. The factor Z_3 is a renormalization constant for the absorbed and emitted photon lines. The Green function $g_{\gamma_f,A';\gamma_i,A}(E',E,k_i^0)$ describes the scattering of a photon by bound electrons, while the Green functions $g_{AA}(E)$ and $g_{A'A'}(E)$ characterize the initial and final bound-electron states. Since the Rayleigh S-matrix element $S^{\rm R}_{\gamma_f,A';\gamma_i,A}$ is expressed in terms of the Green functions, it can be calculated order-by-order by applying the QED perturbation theory with regard to the radiation-matter interaction.

In the following, we shall consider in further detail the nonresonant Rayleigh scattering of light by heliumlike ions, i.e., for photon energies which are not close to possible excitations of any quasistationary bound state. The zeroth-order two-electron wave functions u_A and $u_{A'}$ are constructed as linear combinations of Slater determinants, $A = (a_1,a_2)_{J_A M_A}$ and $A' = (a_1,a_2)_{J_{A'} M_{A'}}$ as

$$\begin{aligned} u_A(\mathbf{r}_1,\mathbf{r}_2) &= F_A \frac{1}{\sqrt{2}} \begin{vmatrix} u_{a_1}(\mathbf{r}_1) & u_{a_2}(\mathbf{r}_1) \\ u_{a_1}(\mathbf{r}_2) & u_{a_2}(\mathbf{r}_2) \end{vmatrix} \\ &= F_A \frac{1}{\sqrt{2}} \sum_P (-1)^P |P a_1 P a_2\rangle, \end{aligned} \quad (5)$$

where F_A is a shorthand notation for the summation over the Clebsch-Gordan coefficients,

$$F_A|a_1a_2\rangle = \sum_{m_{a_1},m_{a_2}} C^{J_A M_A}_{j_{a_1} m_{a_1} j_{a_2} m_{a_2}} |a_1a_2\rangle \times \begin{cases} 1, & a_1 \neq a_2 \\ 1/\sqrt{2}, & a_1 = a_2 \end{cases}, \quad (6)$$

j_a the one-electron total angular momentum and m_a its projection, P is the permutation operator, giving rise to the sign $(-1)^P$ of the permutation for any permutation of the electron coordinates. The same notations hold for the final state A'. The one-electron wave functions u_{a_1} and u_{a_2} are found by solving the Dirac equation with the Coulomb potential of the nucleus.

A. Zeroth-order approximation

In order to calculate the S-matrix element $S^{\mathrm{R}}_{\gamma_f,A';\gamma_i,A}$ of the Rayleigh scattering according to Eq. (4), we decompose the two-time Green functions in a perturbation series with an expansion parameter α and group the terms of the same order together. In zeroth-order approximation, the corresponding Feynman diagrams are depicted in Fig. 1. Then, by employing Eqs. (3) and (4) we obtain the zeroth-order Rayleigh scattering amplitude $\tau^{(0)}_{\gamma_f,A';\gamma_i,A}$ in the following form:

$$\tau^{(0)}_{\gamma_f,A';\gamma_i,A} = \frac{1}{2\pi i}\oint_{\Gamma_A} dE' \oint_{\Gamma_A} dE\, g^{(0)}_{\gamma_f,A';\gamma_i,A}\big(E',E,k_i^0\big), \quad (7)$$

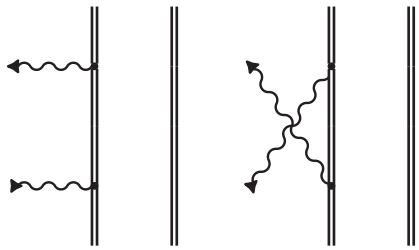

FIG. 1. Feynman diagrams of the Rayleigh scattering in zeroth-order approximation. The double line indicates the electron propagators in the Coulomb field of the nucleus, while the photon absorption and emission are depicted by the wavy line with incoming and outgoing arrows, respectively.

where the superscript "(0)" indicates the order of the perturbation expansion. According to the Feynman rules, the zeroth-order Green function $g^{(0)}_{\gamma_f,A';\gamma_i,A}$ can be written as

$$\begin{aligned}
&g^{(0)}_{\gamma_f,A';\gamma_i,A}\big(E',E,k_i^0\big)\delta\big(E'+k_f^0-k_i^0-E\big)\\
&\quad= F_A F_{A'}\sum_{P,\,Q}(-1)^{P+Q}\int_{-\infty}^{\infty} dp_1^0 dp_2^0 dp_1'^0 dp_2'^0 dq^0\,\delta\big(E-p_1^0-p_2^0\big)\,\delta\big(E'-p_1'^0-p_2'^0\big)\\
&\qquad\times\Bigg\{\langle Pa_1'|\frac{i}{2\pi}\sum_{n_1}\frac{|n_1\rangle\langle n_1|}{p_1'^0-u\varepsilon_{n_1}}\frac{2\pi}{i}R_f^*\delta\big(p_1'^0+k_f^0-q^0\big)\frac{i}{2\pi}\sum_{n_2}\frac{|n_2\rangle\langle n_2|}{q^0-u\varepsilon_{n_2}}\frac{2\pi}{i}R_i\delta\big(q^0-k_i^0-p_1^0\big)\\
&\qquad\times\frac{i}{2\pi}\sum_{n_3}\frac{|n_3\rangle\langle n_3|}{p_1^0-u\varepsilon_{n_3}}|Qa_1\rangle\langle Pa_2'|\frac{i}{2\pi}\sum_{n_4}\frac{|n_4\rangle\langle n_4|}{p_2^0-u\varepsilon_{n_4}}|Qa_2\rangle\delta\big(p_2'^0-p_2^0\big)\\
&\qquad+\langle Pa_1'|\frac{i}{2\pi}\sum_{n_1}\frac{|n_1\rangle\langle n_1|}{p_1'^0-u\varepsilon_{n_1}}\frac{2\pi}{i}R_i\delta\big(p_1'^0-k_i^0-q^0\big)\frac{i}{2\pi}\sum_{n_2}\frac{|n_2\rangle\langle n_2|}{q^0-u\varepsilon_{n_2}}\frac{2\pi}{i}R_f^*\delta\big(q^0+k_f^0-p_1^0\big)\\
&\qquad\times\frac{i}{2\pi}\sum_{n_3}\frac{|n_3\rangle\langle n_3|}{p_1^0-u\varepsilon_{n_3}}|Qa_1\rangle\langle Pa_2'|\frac{i}{2\pi}\sum_{n_4}\frac{|n_4\rangle\langle n_4|}{p_2^0-u\varepsilon_{n_4}}|Qa_2\rangle\delta\big(p_2'^0-p_2^0\big)\Bigg\}\\
&\quad=\frac{i}{2\pi}\frac{\delta\big(E'+k_f^0-k_i^0-E\big)}{\big(E'-E_A^{(0)}\big)\big(E-E_A^{(0)}\big)}F_A F_{A'}\sum_{P,\,Q}(-1)^{P+Q}\sum_n\left\{\frac{\langle Pa_1'|R_f^*|n\rangle\langle n|R_i|Qa_1\rangle\delta_{Pa_2'Qa_2}}{E-\varepsilon_{Qa_2}+k_i^0-u\varepsilon_n}+\frac{\langle Pa_1'|R_i|n\rangle\langle n|R_f^*|Qa_1\rangle\delta_{Pa_2'Qa_2}}{E'-\varepsilon_{Pa_2}-k_i^0-u\varepsilon_n}\right\}.
\end{aligned} \quad (8)$$

$R_f^*(\mathbf{r}) = e\,\boldsymbol{\alpha}\,\boldsymbol{\epsilon}_f^*\,e^{-i\mathbf{k}_f\mathbf{r}}/\sqrt{2k_f^0(2\pi)^3}$ and $R_i(\mathbf{r}) = e\,\boldsymbol{\alpha}\,\boldsymbol{\epsilon}_i\,e^{i\mathbf{k}_i\mathbf{r}}/\sqrt{2k_i^0(2\pi)^3}$ are the emission and absorption operators, $\boldsymbol{\alpha}$ is the vector of the Dirac α matrices, and where the zeroth-order energy of the bound electrons $E_A^{(0)}$ is equal to the sum of the one-electron Dirac energies $E_A^{(0)} = \varepsilon_{a_1} + \varepsilon_{a_2}$. Furthermore, the factor $u = 1 - i0$ in expression (8) preserves the proper treatment of poles of the electron propagators. In the case of the nonresonant scattering, the expressions in the curly brackets of Eq. (8) are regular functions of E and E' as long as $E \approx E_A^{(0)}$ and $E' \approx E_A^{(0)}$. By substituting Eq. (8) into Eq. (7) and by integrating over E and E', one thus easily obtains

$$\begin{aligned}
\tau^{(0)}_{\gamma_f,A';\gamma_i,A} &= -F_A F_{A'}\sum_{P,\,Q}(-1)^{P+Q}\delta_{Pa_2'Qa_2}\sum_n\left\{\frac{\langle Pa_1'|R_f^*|n\rangle\langle n|R_i|Qa_1\rangle}{\varepsilon_{Qa_1}+k_i^0-u\varepsilon_n}+\frac{\langle Pa_1'|R_i|n\rangle\langle n|R_f^*|Qa_1\rangle}{\varepsilon_{Pa_1}-k_i^0-u\varepsilon_n}\right\}\\
&= -F_A F_{A'}\sum_n\left\{\left(\frac{\langle a_1'|R_f^*|n\rangle\langle n|R_i|a_1\rangle}{\varepsilon_{a_1}+k_i^0-u\varepsilon_n}+\frac{\langle a_1'|R_i|n\rangle\langle n|R_f^*|a_1\rangle}{\varepsilon_{a_1}-k_i^0-u\varepsilon_n}\right)\delta_{m_{a_2'}m_{a_2}}\right.\\
&\quad\left.+\left(\frac{\langle a_2'|R_f^*|n\rangle\langle n|R_i|a_2\rangle}{\varepsilon_{a_2}+k_i^0-u\varepsilon_n}+\frac{\langle a_2'|R_i|n\rangle\langle n|R_f^*|a_2\rangle}{\varepsilon_{a_2}-k_i^0-u\varepsilon_n}\right)\delta_{m_{a_1'}m_{a_1}}\right\}.
\end{aligned} \quad (9)$$

Before we shall proceed further, let us discuss this expression for the zeroth-order Rayleigh scattering amplitude $\tau^{(0)}_{\gamma_f,A';\gamma_i,A}$. Obviously, this amplitude splits into two pieces as indicated by the round brackets. These pieces correspond to either the scattering by just the a_1 (first round brackets) or a_2 (second round brackets) electrons. In the zeroth-order approximation, hence, the obtained Rayleigh scattering amplitude corresponds to the IPA formulas as they are widely used for the theoretical description of the Rayleigh scattering; see, e.g., Ref. [22].

Using the (zeroth-order) Rayleigh scattering amplitude from above, the angle-differential Rayleigh scattering cross section defined by Eq. (2) is given in zeroth-order approximation by

$$d\sigma^{(0)}(\mathbf{k}_f;\mathbf{k}_i,\boldsymbol{\epsilon}_i) = \frac{(2\pi)^4\left(k_i^0\right)^2}{2J_A+1}\sum_{M_A,\,M_{A'}}\sum_{\boldsymbol{\epsilon}_f}\left|\tau^{(0)}_{\gamma_f,A';\gamma_i,A}\right|^2 d\Omega_f, \tag{10}$$

while the corresponding zeroth-order total cross section gives rise to

$$\sigma^{(0)}(\mathbf{k}_i,\boldsymbol{\epsilon}_i) = \frac{(2\pi)^4\left(k_i^0\right)^2}{2J_A+1}\sum_{M_A,\,M_{A'}}\sum_{\boldsymbol{\epsilon}_f}\int\left|\tau^{(0)}_{\gamma_f,A';\gamma_i,A}\right|^2 d\Omega_f. \tag{11}$$

In the following, we shall go beyond the zeroth-order approximation and investigate the effects due to the electron-electron correlations. To do so, we need to account for the interelectronic-interaction correction to the Rayleigh scattering amplitude. In the next subsection we now present the corresponding formulas for the first-order interelectronic-interaction effects.

B. First-order interelectronic-interaction correction

In order to obtain the expression for the first-order interelectronic-interaction correction to the Rayleigh S-matrix element, we have to collect all first-order terms in Eq. (4) as they arise from the perturbation expansion of the Green functions. Using Eq. (3), the corresponding interelectronic-interaction correction to the scattering amplitude $\Delta\tau^{(1)}_{\gamma_f,A';\gamma_i,A}$ is given by

$$\begin{aligned}\Delta\tau^{(1)}_{\gamma_f,A';\gamma_i,A} = \frac{1}{2\pi i}\Bigg[&\oint_{\Gamma_A}dE'\oint_{\Gamma_A}dE\;\Delta g^{(1)}_{\gamma_f,A';\gamma_i,A}\left(E',E,k_i^0\right)\\ &-\frac{1}{2}\oint_{\Gamma_A}dE'\oint_{\Gamma_A}dE\;g^{(0)}_{\gamma_f,A';\gamma_i,A}\left(E',E,k_i^0\right)\\ &\times\left(\frac{1}{2\pi i}\oint_{\Gamma_A}dE\;\Delta g^{(1)}_{A'A'}(E)\right.\\ &\left.+\;\frac{1}{2\pi i}\oint_{\Gamma_A}dE\;\Delta g^{(1)}_{AA}(E)\right)\Bigg],\end{aligned} \tag{12}$$

where the first-order interelectronic-interaction correction to the scattering Green function $\Delta g^{(1)}_{\gamma_f,A';\gamma_i,A}$ can be represented by Feynman diagrams as displayed in Fig. 2. The corresponding corrections to the Green functions $\Delta g^{(1)}_{A'A'}$ and $\Delta g^{(1)}_{AA}$ are defined by the first-order interelectronic-interaction diagram shown in Fig. 3. In addition, by making use of the Feynman rules for the two-time Green functions one can derive the final expressions for the scattering amplitude correction $\Delta\tau^{(1)}_{\gamma_f,A';\gamma_i,A}$. This derivation is technically very similar to those as performed in Refs. [33,34], where the interelectronic-interaction effects were investigated for one- and two-photon bound-bound transitions in heliumlike ions. For the sake of brevity, we therefore omit here the cumbersome expressions and go on to the final form of the first-order interelectronic-interaction correction $\Delta\tau^{(1)}_{\gamma_f,A';\gamma_i,A}$ which can be written as the following sum:

$$\begin{aligned}\Delta\tau^{(1)}_{\gamma_f,A';\gamma_i,A} = \Delta\tau^{(1A)}_{\gamma_f,A';\gamma_i,A} + \Delta\tau^{(1B)}_{\gamma_f,A';\gamma_i,A} + \Delta\tau^{(1C)}_{\gamma_f,A';\gamma_i,A}\\ + \Delta\tau^{(1D)}_{\gamma_f,A';\gamma_i,A} + \Delta\tau^{(1R)}_{\gamma_f,A';\gamma_i,A}.\end{aligned} \tag{13}$$

Here, the different contributions are distinguished by the superscripts $(1A)$, $(1B)$, $(1C)$, and $(1D)$ and correspond to the so-called *irreducible* parts of the diagrams as shown in Figs. 2 (a), 2(b), 2(c), and 2(d), respectively. These terms are given by the following expressions:

$$\begin{aligned}\Delta\tau^{(1A)}_{\gamma_f,A';\gamma_i,A} = -F_A F_{A'}\sum_{P,\,Q}(-1)^{P+Q}\sum_{n_1,n_2}^{\varepsilon_{n_2}\neq\varepsilon_{Pa_1}}\Bigg\{&\frac{\langle Pa'_1|R_f^*|n_1\rangle\langle n_1|R_i|n_2\rangle\langle n_2Pa'_2|I\left(\varepsilon_{Pa_2}-\varepsilon_{Qa_2}\right)|Qa_1Qa_2\rangle}{\left(\varepsilon_{Pa_1}+k_i^0-u\varepsilon_{n_1}\right)\left(\varepsilon_{Pa_1}-\varepsilon_{n_2}\right)}\\ &+\frac{\langle Pa'_1|R_i|n_1\rangle\langle n_1|R_f^*|n_2\rangle\langle n_2Pa'_2|I\left(\varepsilon_{Pa_2}-\varepsilon_{Qa_2}\right)|Qa_1Qa_2\rangle}{\left(\varepsilon_{Pa_1}-k_i^0-u\varepsilon_{n_1}\right)\left(\varepsilon_{Pa_1}-\varepsilon_{n_2}\right)}\Bigg\}.\end{aligned} \tag{14}$$

$$\begin{aligned}\Delta\tau^{(1B)}_{\gamma_f,A';\gamma_i,A} = -F_A F_{A'}\sum_{P,\,Q}(-1)^{P+Q}\sum_{n_1,n_2}\Bigg\{&\frac{\langle Pa'_1|R_f^*|n_1\rangle\langle n_1Pa'_2|I\left(\varepsilon_{Pa_2}-\varepsilon_{Qa_2}\right)|n_2Qa_2\rangle\langle n_2|R_i|Qa_1\rangle}{\left(\varepsilon_{Pa_1}+k_i^0-u\varepsilon_{n_1}\right)\left(\varepsilon_{Qa_1}+k_i^0-u\varepsilon_{n_2}\right)}\\ &+\frac{\langle Pa'_1|R_i|n_1\rangle\langle n_1Pa'_2|I\left(\varepsilon_{Pa_2}-\varepsilon_{Qa_2}\right)|n_2Qa_2\rangle\langle n_2|R_f^*|Qa_1\rangle}{\left(\varepsilon_{Pa_1}-k_i^0-u\varepsilon_{n_1}\right)\left(\varepsilon_{Qa_1}-k_i^0-u\varepsilon_{n_2}\right)}\Bigg\},\end{aligned} \tag{15}$$

$$\begin{aligned}\Delta\tau^{(1C)}_{\gamma_f,A';\gamma_i,A} = -F_A F_{A'}\sum_{P,\,Q}(-1)^{P+Q}\sum_{n_1,n_2}^{\varepsilon_{n_1}\neq\varepsilon_{Qa_1}}\Bigg\{&\frac{\langle Pa'_1Pa'_2|I\left(\varepsilon_{Pa_2}-\varepsilon_{Qa_2}\right)|n_1Qa_2\rangle\langle n_1|R_f^*|n_2\rangle\langle n_2|R_i|Qa_1\rangle}{\left(\varepsilon_{Qa_1}-\varepsilon_{n_1}\right)\left(\varepsilon_{Qa_1}+k_i^0-u\varepsilon_{n_2}\right)}\end{aligned}$$

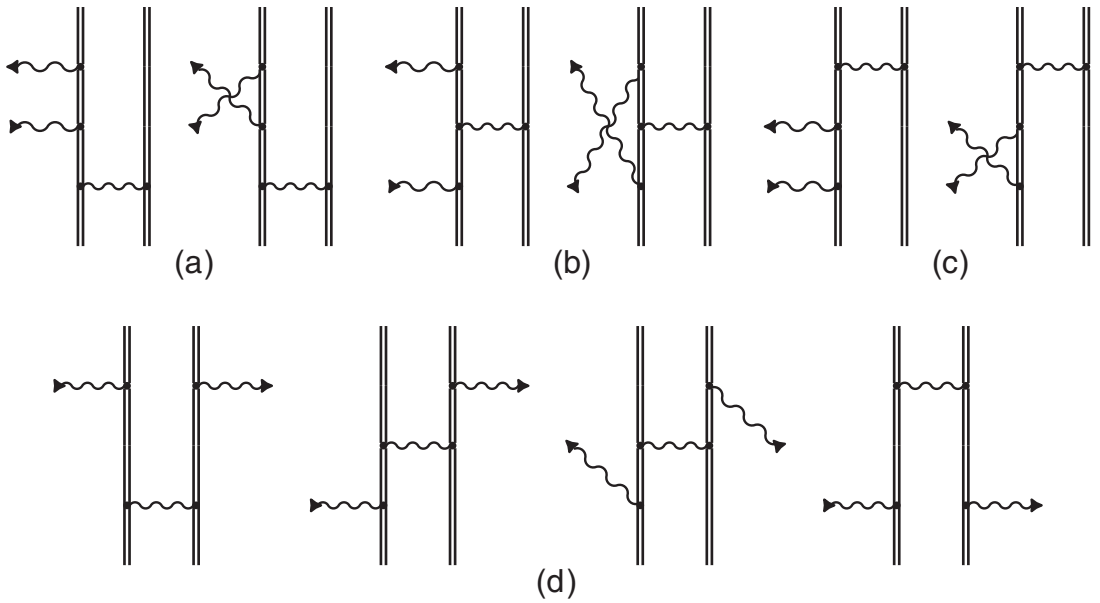

FIG. 2. Feynman diagrams to represent the first-order interelectronic-interaction corrections to the Rayleigh scattering process. The internal wavy line stands for the photon propagator. The rest notations are the same as in Fig. 1.

$$+\frac{\langle Pa_1' Pa_2'|I\left(\varepsilon_{Pa_2}-\varepsilon_{Qa_2}\right)|n_1 Qa_2\rangle\langle n_1|R_i|n_2\rangle\langle n_2|R_f^*|Qa_1\rangle}{\left(\varepsilon_{Qa_1}-\varepsilon_{n_1}\right)\left(\varepsilon_{Qa_1}-k_i^0-u\varepsilon_{n_2}\right)}\Bigg\}, \tag{16}$$

$$\Delta\tau^{(1D)}_{\gamma_f,A';\gamma_i,A} = -F_A F_{A'}\sum_{P,\,Q}(-1)^{P+Q}\sum_{n_1,n_2}\Bigg\{\frac{\langle Pa_1'|R_i|n_1\rangle\langle Pa_2'|R_f^*|n_2\rangle\langle n_1 n_2|I\left(k_i^0-\varepsilon_{Pa_1}+\varepsilon_{Qa_1}\right)|Qa_1 Qa_2\rangle}{\left(\varepsilon_{Pa_1}-k_i^0-u\varepsilon_{n_1}\right)\left(\varepsilon_{Pa_2}+k_i^0-u\varepsilon_{n_2}\right)}$$

$$+\frac{\langle Pa_1' n_2|I\left(k_i^0-\varepsilon_{Pa_1}+\varepsilon_{Qa_1}\right)|n_1 Qa_2\rangle\langle Pa_2'|R_f^*|n_2\rangle\langle n_1|R_i|Qa_1\rangle}{\left(\varepsilon_{Qa_1}+k_i^0-u\varepsilon_{n_1}\right)\left(\varepsilon_{Pa_2}+k_i^0-u\varepsilon_{n_2}\right)}$$

$$+\frac{\langle Pa_1' n_2|I\left(k_i^0+\varepsilon_{Pa_1}-\varepsilon_{Qa_1}\right)|n_1 Qa_2\rangle\langle Pa_2'|R_i|n_2\rangle\langle n_1|R_f^*|Qa_1\rangle}{\left(\varepsilon_{Qa_1}-k_i^0-u\varepsilon_{n_1}\right)\left(\varepsilon_{Pa_2}-k_i^0-u\varepsilon_{n_2}\right)}$$

$$+\frac{\langle Pa_1' Pa_2'|I\left(k_i^0-\varepsilon_{Pa_1}+\varepsilon_{Qa_1}\right)|n_1 n_2\rangle\langle n_1|R_i|Qa_1\rangle\langle n_2|R_f^*|Qa_2\rangle}{\left(\varepsilon_{Qa_1}+k_i^0-u\varepsilon_{n_1}\right)\left(\varepsilon_{Qa_2}-k_i^0-u\varepsilon_{n_2}\right)}\Bigg\}, \tag{17}$$

and where $I(\omega)=e^2\alpha^\mu\alpha^\nu D_{\mu\nu}(\omega)$ refers to the interelectronic-interaction operator with the photon propagator $D_{\mu\nu}(\omega)$. The diagrams displayed in Figs. 2(a) and 2(c) contain also the so-called *reducible* parts, while this is not the case for the diagrams shown in Figs. 2(b) and 2(d). Thus, the last term in Eq. (13) $\Delta\tau^{(1R)}_{\gamma_f,A';\gamma_i,A}$ is the total reducible contribution, which arises from the second term in the square brackets of Eq. (12) and from the reducible parts of the diagrams Figs. 2(a) and 2(c). The total reducible term can be written as

$$\Delta\tau^{(1R)}_{\gamma_f,A';\gamma_i,A} = F_A F_{A'}\sum_{P,\,Q}(-1)^{P+Q}\delta_{Pa_2' Qa_2}\sum_n\Bigg\{\left(\frac{\langle Pa_1'|R_f^*|n\rangle\langle n|R_i|Qa_1\rangle}{\left(\varepsilon_{Qa_1}+k_i^0-u\varepsilon_n\right)^2}+\frac{\langle Pa_1'|R_i|n\rangle\langle n|R_f^*|Qa_1\rangle}{\left(\varepsilon_{Pa_1}-k_i^0-u\varepsilon_n\right)^2}\right)\Delta E_A^{(1)}$$

$$+\left(\frac{\langle Pa_1'|R_f^*|n\rangle\langle n|R_i|Qa_1\rangle}{\varepsilon_{Qa_1}+k_i^0-u\varepsilon_n}+\frac{\langle Pa_1'|R_i|n\rangle\langle n|R_f^*|Qa_1\rangle}{\varepsilon_{Pa_1}-k_i^0-u\varepsilon_n}\right)\Delta E_A^{\prime(1)}\Bigg\}, \tag{18}$$

where

$$\Delta E_A^{(1)} = F_A F_{\tilde{A}}\sum_P(-1)^P\langle P\tilde{a}_1 P\tilde{a}_2|I(\varepsilon_{P\tilde{a}_1}-\varepsilon_{a_1})|a_1 a_2\rangle \tag{19}$$

is the one-photon exchange correction and

$$\Delta E_A^{\prime(1)} = F_A F_{\tilde{A}}\sum_P(-1)^P\langle P\tilde{a}_1 P\tilde{a}_2|\frac{dI(x)}{dx}\Big|_{\Delta=\varepsilon_{P\tilde{a}_1}-\varepsilon_{a_1}}|a_1 a_2\rangle \tag{20}$$

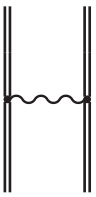

FIG. 3. One-photon exchange Feynman diagram. Notations are the same as in Figs. 1 and 2.

is the first-order derivative of the one-photon exchange correction.

Finally, the angle-differential Rayleigh scattering cross section up to the first order in the interelectronic interaction is given by

$$d\sigma^{(1)}(\mathbf{k}_f;\mathbf{k}_i,\boldsymbol{\epsilon}_i) = \frac{(2\pi)^4\left(k_i^0\right)^2}{2J_A+1}\sum_{M_A,\,M_{A'}}\sum_{\boldsymbol{\epsilon}_f}\left|\tau^{(0)}_{\gamma_f,A';\gamma_i,A} + \Delta\tau^{(1)}_{\gamma_f,A';\gamma_i,A}\right|^2 d\Omega_f, \tag{21}$$

while the corresponding total cross section takes the form,

$$\sigma^{(1)}(\mathbf{k}_i,\boldsymbol{\epsilon}_i) = \frac{(2\pi)^4\left(k_i^0\right)^2}{2J_A+1}\sum_{M_A,\,M_{A'}}\sum_{\boldsymbol{\epsilon}_f}\int\left|\tau^{(0)}_{\gamma_f,A';\gamma_i,A} + \Delta\tau^{(1)}_{\gamma_f,A';\gamma_i,A}\right|^2 d\Omega_f. \tag{22}$$

These Rayleigh scattering cross sections take rigorously into account the many-electron effects on a level of the one-photon exchange. These calculations enable us to analyze systematically the importance of the many-electron effects upon the elastic scattering cross sections. However, before we continue with this analysis let us consider a different approach for including the many-electron effects in the next subsection.

C. Screening potential approximation

Apart from the rigorous approach above, the zeroth-order or independent-particle approximation of Eq. (9) also facilitates a partial account of the interelectronic-interaction effects in the Rayleigh cross sections. To this end, we shall start from an extended Furry picture in which a central screening potential is incorporated into the zeroth-order Hamiltonian. In this case, the formula (9) for the zeroth-order Rayleigh amplitude remains formally the same, while the initial, intermediate, and final one-electron wave functions are now generated within a *mean-field* potential by including, in addition to the Coulomb field, also some screening potential. In practice, however, this approach only includes some (major) parts of the many-electron effects for highly charged ions. Here, we shall separate this part from the complete first-order result in Eq. (13) by restricting ourselves to the static Coulomb part in the photon propagator $D_{\mu\nu}$ as well as to the spherical terms in its multipole expansion. Below, we shall refer to this approximation by the superscript "scr" in the Rayleigh scattering amplitude,

$$\Delta\tau^{(1)\mathrm{scr}}_{\gamma_f,A';\gamma_i,A} = \Delta\tau^{(1A)\mathrm{scr}}_{\gamma_f,A';\gamma_i,A} + \Delta\tau^{(1B)\mathrm{scr}}_{\gamma_f,A';\gamma_i,A} + \Delta\tau^{(1C)\mathrm{scr}}_{\gamma_f,A';\gamma_i,A} + \Delta\tau^{(1R)\mathrm{scr}}_{\gamma_f,A';\gamma_i,A}. \tag{23}$$

Let us mention here that the contribution of the diagrams in Fig. 2(d) should also be excluded in this case since these diagrams are of inherent many-electron character. In the leading order this approximation is equivalent to the IPA with the Dirac-Hartree-Fock potential. The difference arisen from the higher-order terms can be neglected for highly charged ions.

With these "screening" corrections to the Rayleigh scattering amplitude, the angle differential and total cross sections take now the form,

$$d\sigma^{\mathrm{scr}}(\mathbf{k}_f;\mathbf{k}_i,\boldsymbol{\epsilon}_i) = \frac{(2\pi)^4\left(k_i^0\right)^2}{2J_A+1}\sum_{M_A,\,M_{A'}}\sum_{\boldsymbol{\epsilon}_f}\left|\tau^{(0)}_{\gamma_f,A';\gamma_i,A} + \Delta\tau^{(1)\mathrm{scr}}_{\gamma_f,A';\gamma_i,A}\right|^2 d\Omega_f, \tag{24}$$

and

$$\sigma^{\mathrm{scr}}(\mathbf{k}_i,\boldsymbol{\epsilon}_i) = \frac{(2\pi)^4\left(k_i^0\right)^2}{2J_A+1}\sum_{M_A,\,M_{A'}}\sum_{\boldsymbol{\epsilon}_f}\int\left|\tau^{(0)}_{\gamma_f,A';\gamma_i,A} + \Delta\tau^{(1)\mathrm{scr}}_{\gamma_f,A';\gamma_i,A}\right|^2 d\Omega_f, \tag{25}$$

respectively. Since this approximation can be obtained from Eq. (9) by just making use of a screening potential in solving the Dirac equation, we shall refer to it as the IPA. In the next section, we now discuss the numerical procedure and the methods employed in the computation of the cross sections.

III. COMPUTATIONS

The formulas (9), (13), and (23) for the transition amplitudes, as obtained in the previous section, require further simplifications to make detailed computations feasible. For instance, in order to perform the angular integrations in the one- and two-electron matrix elements, we utilize the well-known multipole expansion technique. Indeed, this angular integration can be carried out analytically by expanding the transition operators R_f^* and R_i as well as the photon propagator $D_{\mu\nu}$ in multipole series. For the sake of brevity, we do not recall the corresponding expressions here and just refer the reader to the literature for further details [35]. The infinite multipole summations over the incoming and outgoing photon multipoles are further restricted by analyzing the convergence and more often than not we summed up to 10 multipoles.

Numerically most demanding in the computations is the infinite summation over the complete Dirac spectrum n_1 and n_2, which not only contain the bound states but also the positive- and negative-energy Dirac continuum. In order to perform such a summation several independent approaches were employed previously in the consideration of the Rayleigh scattering. One method formulated in Ref. [14] is based on a solution of an inhomogeneous Dirac equation, a method that was found quite successful and was utilized in a good number of calculations of the elastic scattering cross sections [15–21]. Another approach is known as the finite basis-set method. This technique enables one to replace an infinite summation in the spectral representation of the electron propagator by a summation over a finite basis set and was utilized for calculating the Rayleigh scattering in Refs. [24,27]. Still another approach is based on the exact Dirac-Coulomb Green's

function which can be represented in a closed form as a superposition of the regular and irregular solutions of the Dirac equation. In the case of a pointlike Coulomb potential, for example, it can be expressed analytically [36]. In Refs. [25,26] this method was also utilized in the calculation of the Rayleigh scattering cross sections.

In the present work, we made use of the two latter approaches: the finite basis-set method and the Dirac-Coulomb Green's function. The finite basis set was constructed from B splines [37] by employing the dual-kinetic-balance approach [38]. In addition, the analytic Dirac-Coulomb Green's function for a pointlike Coulomb potential was employed in terms of the Whittaker functions [39]. The finite basis set method enables us to considerably reduce the numerical effort in the calculations. The reason for this is the separation of the radial variables and the subsequent integrations of the single radial integrals. However, when the energies of the incident photons are larger than the ionization threshold, the application of the finite basis-set technique is critically hampered in some of the terms (diagrams). For example, this is the case for the first term of Eq. (9) with the denominator $(\varepsilon_{Qa_1} + k_i^0 - u\varepsilon_n)$. This term has a pole in the energy continuum (spectrum) at $\varepsilon_n = \varepsilon_{Qa_1} + k_i^0 + i0$ that cannot be treated accurately in any finite basis-set method due to the discretized spectrum and the summation over just a finite number of basis functions. In contrast, the use of the Dirac-Coulomb Green's function is free of such difficulties as it represents the exact electron propagator. Therefore, all the electron propagators with energies $\varepsilon_{a_1} + k_i^0$ or $\varepsilon_{a_2} + k_i^0$ were treated by means of the Dirac-Coulomb Green's function G_{κ_n}:

$$\sum_n \frac{|n\rangle\langle n|}{\varepsilon_a + k_i^0 - u\varepsilon_n} \equiv \sum_{n_r,\kappa_n} \frac{u_{n_r\kappa_n}(\mathbf{r}_1)u^\dagger_{n_r\kappa_n}(\mathbf{r}_2)}{\varepsilon_a + k_i^0 - u\varepsilon_{n_r\kappa_n}} = \sum_{\kappa_n} G_{\kappa_n}(\varepsilon_a + k_i^0, \mathbf{r}_1, \mathbf{r}_2), \quad (26)$$

and where n_r and κ_n denote the principal and Dirac angular quantum numbers, respectively. For all other propagators, the finite basis set representation was employed. This combination of different (numerical) techniques enables us to substantially reduce the computational time, while we still obtain (very) accurate results.

Still, a quite serious problem occurs for those terms where *two* Dirac-Coulomb Green's functions appear in the calculations. For example, such a term is the first contribution in Eq. (15) which can be rewritten by means of the Dirac-Coulomb Green's functions as

$$\begin{aligned}\tau^{(1B)}_{\gamma_f,A';\gamma_i,A} = -F_A F_{A'} \sum_{P,Q}(-1)^{P+Q} \sum_{\kappa_{n_1},\kappa_{n_2}} & \\ \times \int d\mathbf{r}_1 d\mathbf{r}_2 d\mathbf{r}_3 d\mathbf{r}_4\, u^\dagger_{Pa_1'}(\mathbf{r}_1) u^\dagger_{Pa_2'}(\mathbf{r}_4) R^*_f(\mathbf{r}_1) & \\ \times G_{\kappa_{n_1}}\left(\varepsilon_{Pa_1} + k_i^0, \mathbf{r}_1, \mathbf{r}_2\right) I(\varepsilon_{Pa_2} - \varepsilon_{Qa_2}, \mathbf{r}_2, \mathbf{r}_4) & \\ \times G_{\kappa_{n_2}}(\varepsilon_{Qa_1} + k_i^0, \mathbf{r}_2, \mathbf{r}_3) R_i(\mathbf{r}_3) u_{Qa_1}(\mathbf{r}_3) u_{Qa_1}(\mathbf{r}_4) & \\ + \text{second term}. \quad (27)\end{aligned}$$

Here, the integration over the $\mathbf{r}_2$ coordinate involves the two Dirac-Coulomb Green's functions $G_{\kappa_{n_1}}(\varepsilon_{Pa_1} + k_i^0, \mathbf{r}_1, \mathbf{r}_2)$ and $G_{\kappa_{n_2}}(\varepsilon_{Qa_1} + k_i^0, \mathbf{r}_2, \mathbf{r}_3)$, and together with the photon propagator $I(\varepsilon_{Pa_2} - \varepsilon_{Qa_2}, \mathbf{r}_2, \mathbf{r}_4)$. In contrast to the integrations over the coordinates $\mathbf{r}_1$, $\mathbf{r}_3$, and $\mathbf{r}_4$, no bound-electron wave function is involved here. Therefore, the integral over r_2 converges only very slowly for large values of r_2, and this makes a straightforward numerical integration extremely cumbersome. For this reason, we here applied the method of the complex-plane rotation of the coordinate integration contour and which was previously used in studying bremsstrahlung [40] and double photoionization processes [41]. We have introduced the radius of the atom R, i.e., a radius outside of which all the bound-state electron wave functions vanish. In the integrals over r_1, r_3, and r_4 we then set the upper bound to R and split the remaining over r_2 into two domains $[0, R]$ and $[R, R - i\infty)$. With these rearrangements in the integration procedure, the integral over the second domain decays exponentially and does no longer cause any (numerical) problem.

In order to check the consistency of our numerical results we have performed calculations in different gauges, namely in length and velocity gauge for the photon wave functions and in Coulomb and Feynman gauge of the photon propagator. The obtained results were found in perfect agreement, independently of the chosen gauge form.

IV. RESULTS AND DISCUSSION

Although the formulas in Sec. II apply generally for heliumlike ions, independent of their particular state, detailed calculations have been performed here only for the Rayleigh scattering by such ions in their $1s^2\ {}^1S_0$ ground state. In particular, we here aim to investigate the "many-electron" effects beyond the IPA, for which two sets of calculations were carried out: a first one, in which the zeroth-order approximation with the Coulomb wave functions were applied in Eqs. (10) and (11) and to which we refer below as the Coulomb results. A second IPA computation was carried out by using the screening potential approximation and Eqs. (24) and (25); these computations are referred to as the screening results. Both of these IPA calculations are compared with the complete zeroth- and first-order results as obtained by means of Eqs. (21) and (22), called the many-electron treatment below.

Figure 4 displays the total cross section for the Rayleigh scattering of light by heliumlike Ni^{26+} ($Z = 28$), Xe^{52+} ($Z = 54$), and Au^{77+} ($Z = 79$) ions and as function of the photon energy. Results are shown for photon energies well above the ionization threshold and for the three computations above: Coulomb $\sigma^{(0)}$, screening $\sigma^{\rm scr}$, and many-electron $\sigma^{(1)}$. To make the differences in the theoretical predictions more explicit, the relative deviations (in %) with regard to the many-electron data are also shown in the lower panel of this figure: $\Delta_\sigma^{(0)} = (\sigma^{(0)} - \sigma^{(1)})/\sigma^{(1)}$ and $\Delta_\sigma^{\rm scr} = (\sigma^{\rm scr} - \sigma^{(1)})/\sigma^{(1)}$. As seen from this figure, all three computations give quite similar results with slightly larger deviations near the ionization threshold. At the threshold, the Rayleigh scattering cross sections appear to be very sensitive due to differences in the calculated threshold energies in the three approximations. For the scattering on heliumlike Au^{77+} ions, for example, the calculated threshold energies are 93.411 keV, 91.857 keV, and 91.656 keV for the Coulomb, screening, and the many-electron computations, respectively. While, in the Coulomb approximation, the

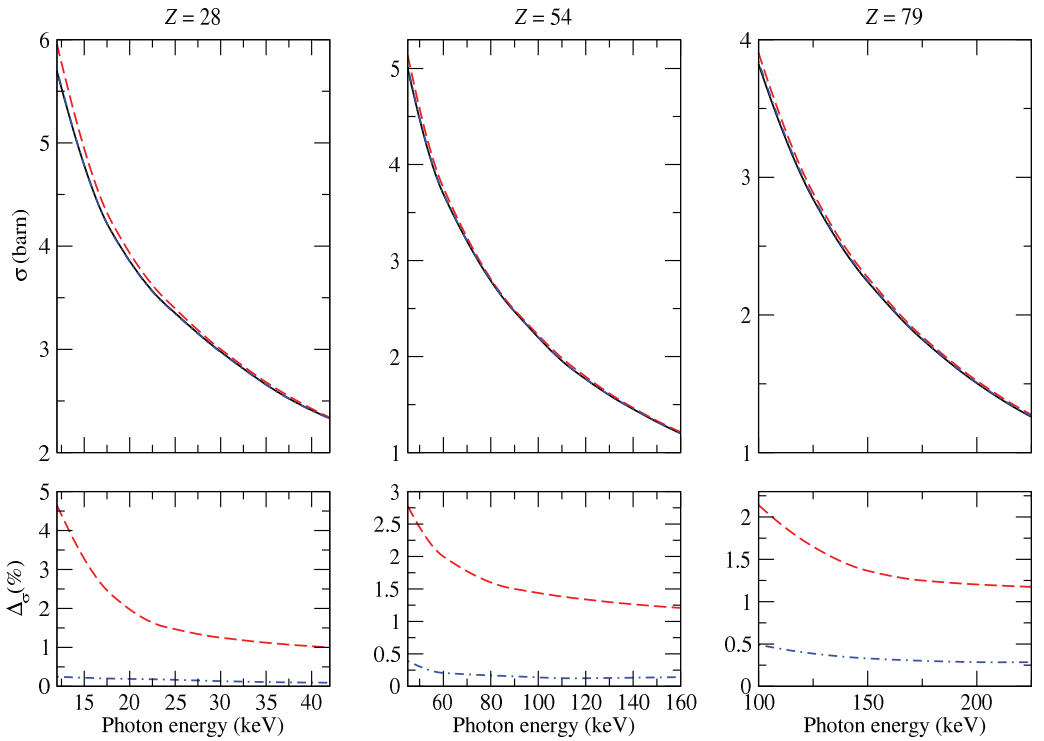

FIG. 4. Total cross section for the Rayleigh scattering of x rays by heliumlike Ni^{26+} ($Z = 28$), Xe^{52+} ($Z = 54$), and Au^{77+} ($Z = 79$) ions in their $^1S_0$ ground state and as function of the photon energy. Predictions are compared for three different approximations in the evaluation of the scattering amplitudes: a pure Coulomb potential $\sigma^{(0)}$ (red dashed line), use of a screening potential $\sigma^{\rm scr}$ (blue dash-dotted line), as well as by applying the full many-electron procedure in $\sigma^{(1)}$ (black solid line). The lower panel displays the differences (in %) between the Coulomb $\Delta_\sigma^{(0)}$ (red dashed line) and the screening cross sections $\Delta_\sigma^{\rm scr}$ (blue dash-dotted line), each relative to the many-electron computations.

ionization threshold is completely determined by the one-electron Dirac binding energy, the interelectronic interactions modify this value in the screening and many-electron calculations. The difference between the ionization energies in the screening and many-electron approximation is due to the contribution of the Breit interaction to the ground-state energy. Thus, the behavior of the differences $\Delta_\sigma^{(0)}$ and $\Delta_\sigma^{\rm scr}$ near the ionization threshold as a function of the nuclear charge can be understood from the ratio of the one-photon exchange and Breit interaction contribution to the threshold energy, respectively. The first ratio decreases while the second one increases with increasing nuclear charge. For large photon energies, all approximations slowly converge each other. This behavior was expected at high energies [22] since the binding effects become less and less important with increasing of the energy of scattered photon. The similar finding was also obtained for the case of the helium atom in Ref. [28].

In addition to the total cross sections, we shall now investigate the angular distribution of the scattered photons and for which we need to fix a geometry for describing the scattering process [cf. Fig. 5]. In the Furry picture, as mentioned above, we can treat the photon scattering in the rest frame of the nucleus, taken as the origin of the coordinates. Moreover, we can choose the z axis along the wave vector $\mathbf{k}_i$ of the incident radiation. Than the scattered photon wave vector $\mathbf{k}_f$ is completely described by the two angles: azimuthal θ and polar ϕ. What concerns the polarization of the incident photon, we consider here two scenarios. In the first scenario the incoming light is completely unpolarized, and the angular distribution is independent on the polar angle ϕ. In the second scenario the incoming light is completely linearly polarized along the x axis; then one observes a dependence of the scattering cross section on the polar angle ϕ as well. Here, we restrict ourselves to the geometry when the photon is observed at the angle $\phi = 0$, thus, defining the reaction plane to be the xz plane.

In Figs. 6 and 7, we display the angle-differential cross sections for the Rayleigh scattering of unpolarized and linearly polarized incoming light, if scattered by heliumlike Ni^{26+} ions

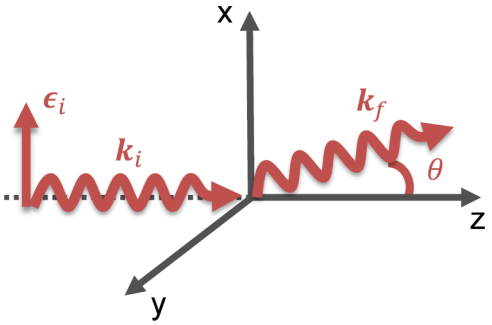

FIG. 5. Geometry for describing the Rayleigh scattering of photons at a nucleus which is taken as the origin of the coordinates. The z axis is chosen along the direction of the incoming light, while the reaction plane is defined by the xz plane. The scattering angle θ then uniquely defines the direction of the scattered photon within the reaction plane.

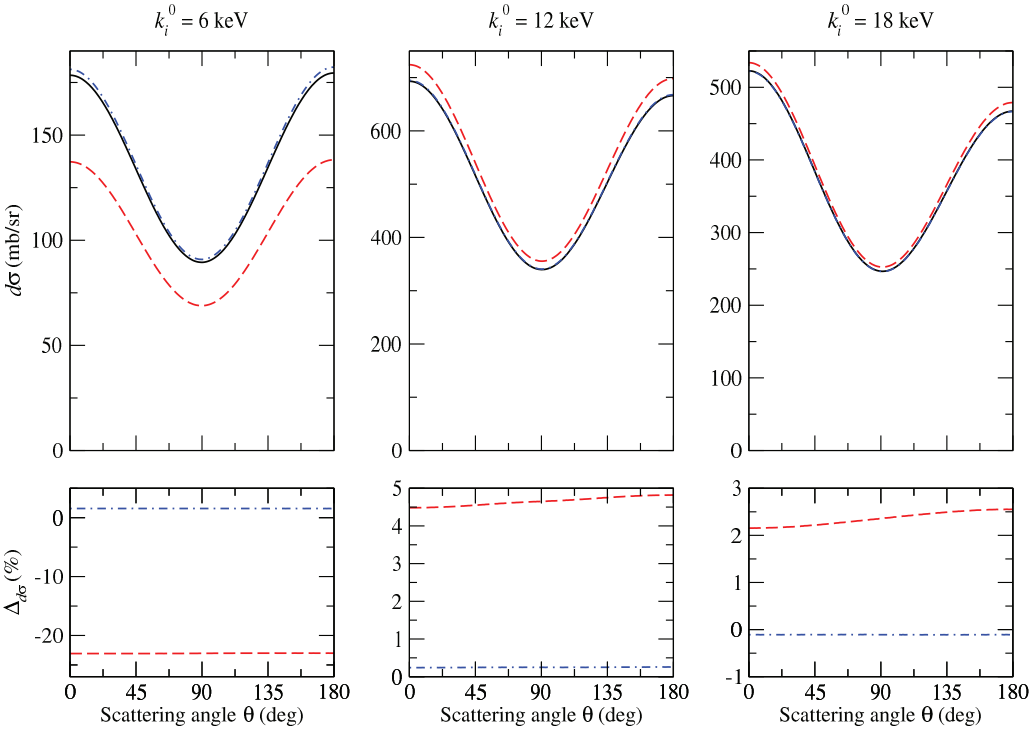

FIG. 6. Angle-differential cross section for the Rayleigh scattering of unpolarized incoming photons with energies $k_i^0 = 6$ keV (left column), $k_i^0 = 12$ keV (middle column), and $k_i^0 = 18$ keV (right column) by heliumlike Ni^{26+} ions in their ground state. Theoretical results are shown for the three approximations in this work: Coulomb $d\sigma^{(0)}$ (red dashed line), screening $d\sigma^{\rm scr}$ (blue dash-dotted line), as well as the many-electron computations $d\sigma^{(1)}$ (black solid line). In the lower panel, again the differences (in %) between the Coulomb $\Delta_{d\sigma}^{(0)}$ (red dashed line) and screening $\Delta_{d\sigma}^{\rm scr}$ results (blue dash-dotted line) are shown, just relative to the many-electron computations.

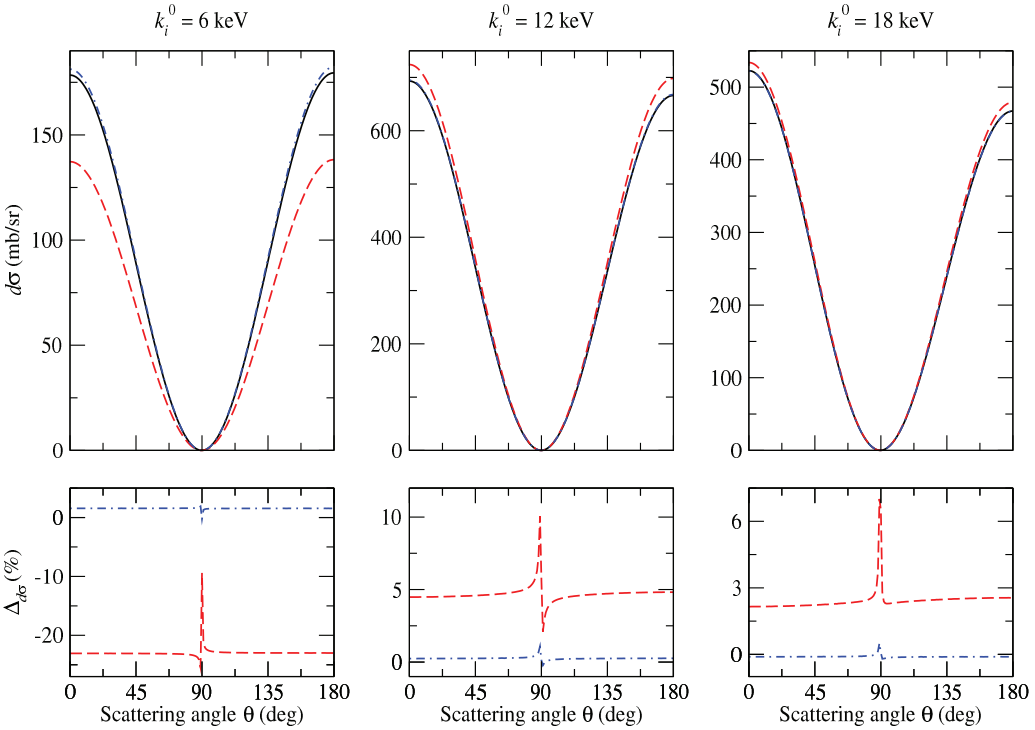

FIG. 7. The same as Fig. 6 but for linearly polarized incoming photons.

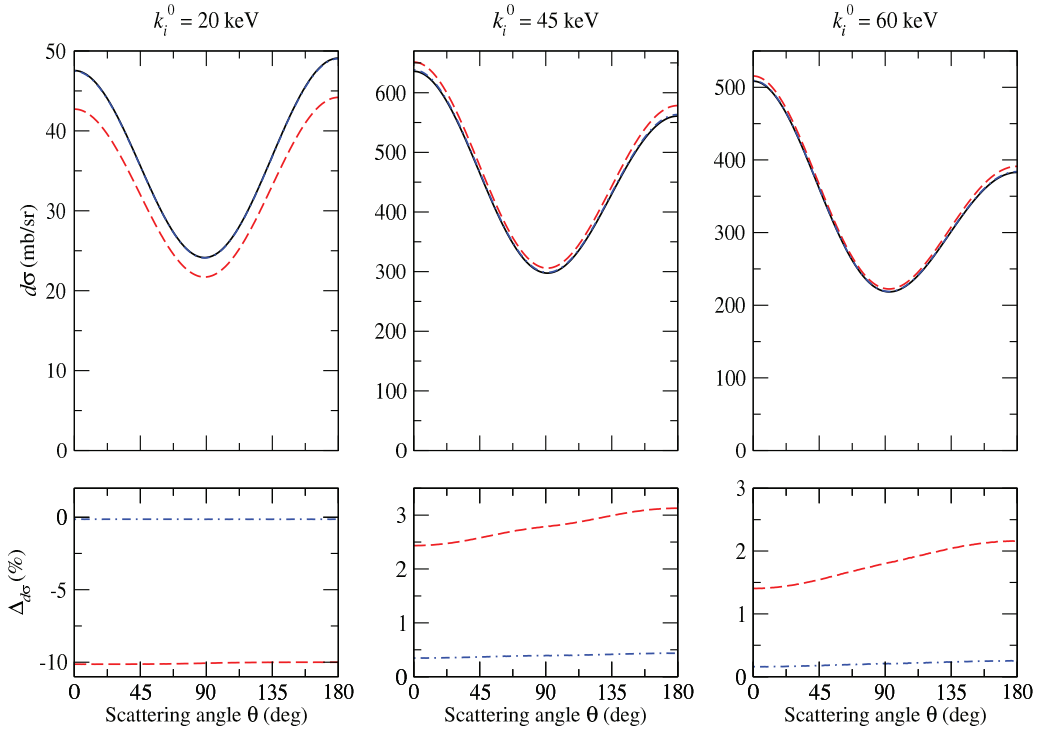

FIG. 8. The same as Fig. 6 but for the Rayleigh scattering by heliumlike Xe^{52+} ions and for incident photon energies $k_i^0 = 20$ keV (left column), $k_i^0 = 45$ keV (middle column), and $k_i^0 = 60$ keV (right column), respectively.

in their ground state. Analog computations were performed also for heliumlike Xe^{26+} and Au^{77+} ions and are given in Figs. 8–11, respectively. These angular distributions of the Rayleigh-scattered photons are shown for three energies of the incoming photons, namely for about half of the ionization threshold as well as for photon energies that are 10% and 50% larger that this threshold. A different behavior of the angular distributions for a different polarization of the incident light can be expected already from the nonrelativistic electric-dipole approximation which predicts a $1 + \cos^2\theta$ shape for

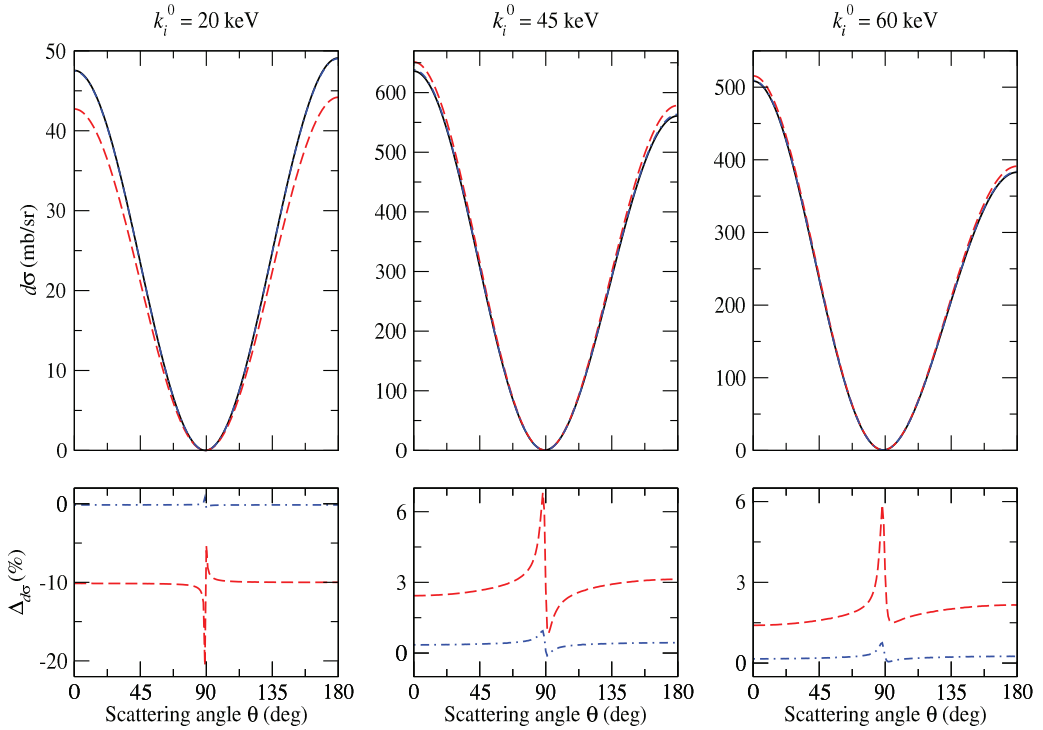

FIG. 9. The same as Fig. 8 but for linearly polarized incoming photons.

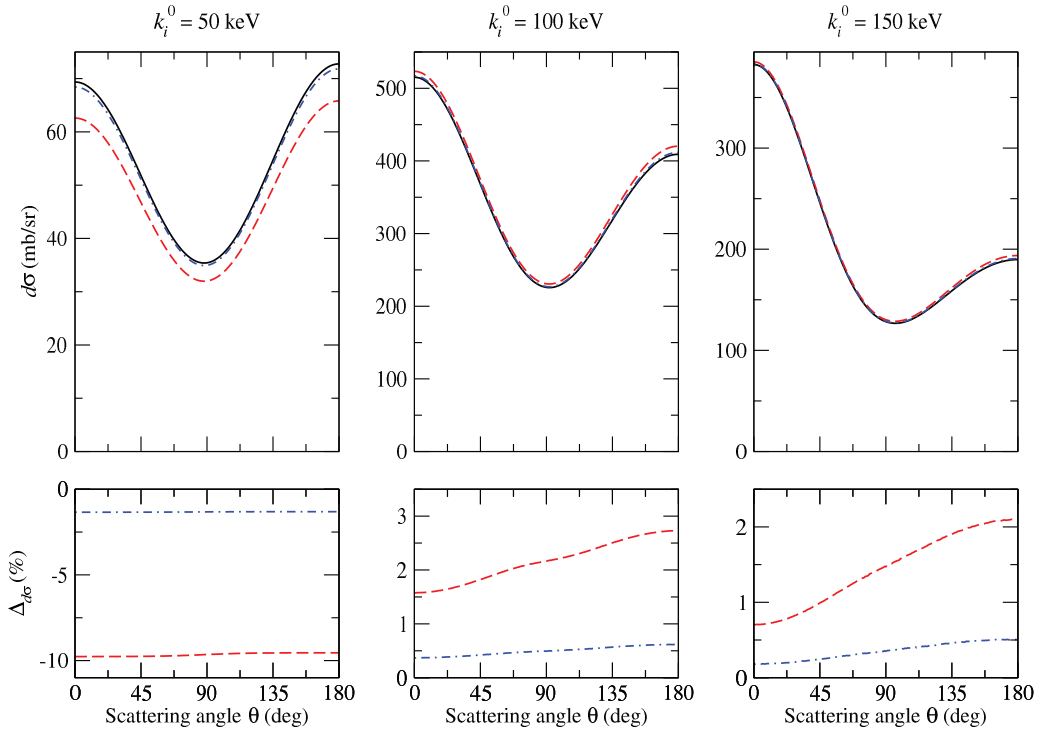

FIG. 10. The same as Fig. 6 but for the Rayleigh scattering by heliumlike Au^{77+} ions and for incident photon energies $k_i^0 = 50$ keV (left column), $k_i^0 = 100$ keV (middle column), and $k_i^0 = 150$ keV (right column), respectively.

unpolarized (incoming) light and a $\cos^2\theta$ shape for completely polarized radiation, respectively. For large photon energies, however, *nondipole* effects become also important and lead to (more or less) strong deviations from this electric-dipole behavior above [13].

Similar as for the total Rayleigh cross sections, we have analyzed and compare in Figs. 6–11 the angle-differential cross sections in the three approximations above: Coulomb $d\sigma^{(0)}$, screening $d\sigma^{\rm scr}$, and many-electron $d\sigma^{(1)}$. Since the deviations between the different computations are typically

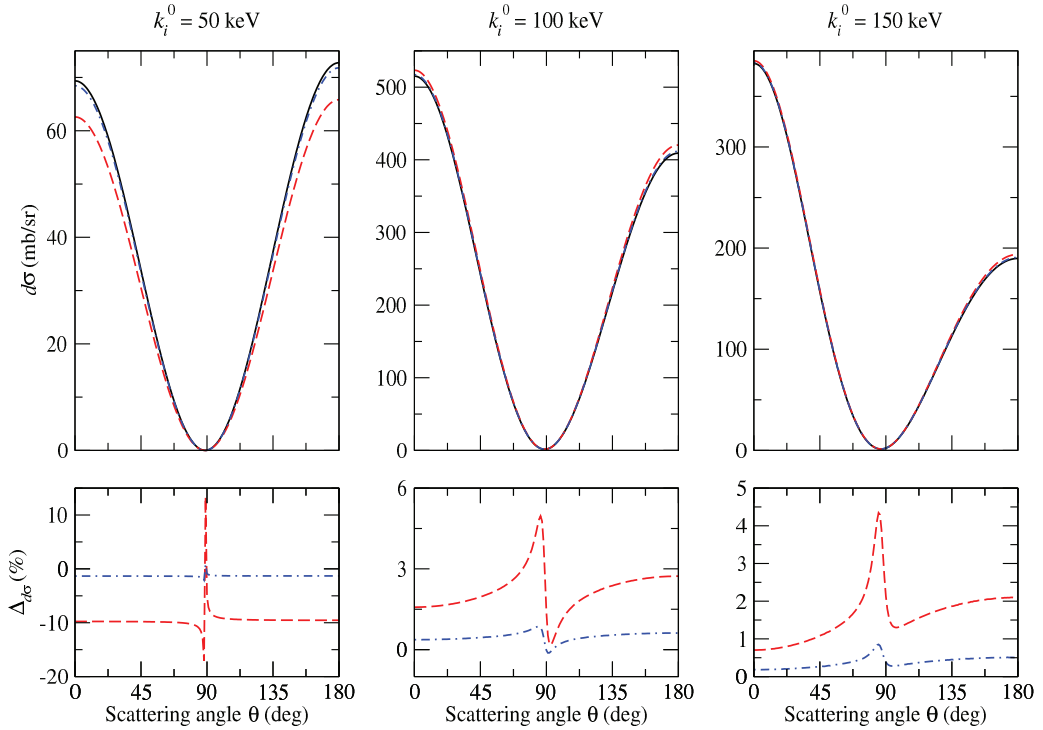

FIG. 11. The same as Fig. 10 but for linearly polarized incoming photons.

small over a wide range of angle, we also display the relative differences, $\Delta_{d\sigma}^{(0)} = (d\sigma^{(0)} - d\sigma^{(1)})/d\sigma^{(1)}$ and $\Delta_{d\sigma}^{\rm scr} = (d\sigma^{\rm scr} - d\sigma^{(1)})/d\sigma^{(1)}$, i.e., normalized to the many-electron data as our best approximation. These relative differences are shown in the lower panels of these figures. While these differences are typically small for energies well above the ionization threshold (in the right columns of these figures), sizable deviations arise below this threshold, and especially for the Coulomb results. The relative differences are large at low Z and clearly demonstrate the importance of the interelectronic-interaction effects. The deviations are, however, less significant between the screening and many-electron computations, i.e., less than 2% for all the cases considered here. This demonstrates that the interelectronic-interaction effects can be treated quite efficiently within the IPA with a screening potential for the case of the Rayleigh scattering of photons on heliumlike ions in their ground state.

V. SUMMARY AND OUTLOOK

In summary, a systematic QED treatment has been presented for the first-order corrections of the interelectronic interaction to the Rayleigh scattering of photons by heliumlike ions. By applying and comparing three different theoretical and computational approaches, we rigorously explore the role of the many-electron effects beyond the IPA to the Rayleigh scattering by highly charged ions. Detailed calculations for the total and angle-differential cross sections were evaluated for the scattering by heliumlike Ni^{26+}, Xe^{52+}, and Au^{77+} ions in their $1s^2\ {}^1S_0$ ground state and, especially, for unpolarized and completely polarized incident radiation. We here found that the interelectronic-interaction effects are more important for photon energies below and just above the ionization threshold. However, the major part of these many-electron contributions can be taken into account by IPA calculations with a screening potential.

For photon energies well above the valence and subvalence binding energies, this conclusion can be generalized also towards more complex atoms. For such atoms and ions, the Rayleigh scattering is typically dominated by the scattering from the inner-shell electrons. However, for photon energies compared with the valence and subvalence binding energies, the Rayleigh scattering cross sections are strongly affected by the scattering from the outer-shell electrons and further care has to be taken in employing the IPA. This can be proven for forward emissions ($\theta = 0$), where the Rayleigh scattering cross section can be related to the photoionization cross section via the dispersion relation and the optical theorem [42]. In complex atoms the photoionization cross section near the ionization threshold often shows various structures, such as the Cooper minima and resonances due to inner-shell excitations, which appear to be very sensitive to many-electron effects. These electronic-structure phenomena will likely affect also the Rayleigh scattering cross sections, especially, for the cases of the scattering by the open-shell electrons [43]. The theoretical formalism above can be applied to such open-shell atoms, although (much) further effort will be needed for its efficient numerical implementation.

ACKNOWLEDGMENTS

This work has been supported by the BMBF (Grant No. 05K13VHA) and RFBR (Grant No. 16-02-00538). V.A.Y. acknowledges support from the Ministry of Education and Science of Russian Federation (program for organizing and carrying out scientific investigations).

[1] M. Y. Sfeir, F. Wang, L. Huang, C.-C. Chuang, J. Hone, S. P. O'Brien, T. F. Heinz, and L. E. Brus, Science **306**, 1540 (2004).
[2] N. S. Kampel, A. Griesmaier, M. P. Hornbak Steenstrup, F. Kaminski, E. S. Polzik, and J. H. Müller, Phys. Rev. Lett. **108**, 090401 (2012).
[3] L. V. Kulik, K. Ovchinnikov, A. S. Zhuravlev, V. E. Bisti, I. V. Kukushkin, S. Schmult, and W. Dietsche, Phys. Rev. B **85**, 113403 (2012).
[4] W. Wu, J. Yue, D. Li, X. Lin, F. Zhu, X. Yin, J. Zhu, X. Dai, P. Liu, Y. Wei *et al.*, Nano Res. **8**, 303 (2015).
[5] K. Maeda, Y. Terada, D. Kasen, F. K. Röpke, A. Bamba, R. Diehl, K. Nomoto, M. Kromer, I. R. Seitenzahl, H. Yamaguchi *et al.*, Astrophys. J. **760**, 54 (2012).
[6] L.-S. The and A. Burrows, Astrophys. J. **786**, 141 (2014).
[7] X.-D. Zhang, D. Wu, X. Shen, J. Chen, Y.-M. Sun, P.-X. Liu, and X.-J. Liang, Biomaterials **33**, 6408 (2012).
[8] S. Fritzsche, P. Indelicato, and T. Stöhlker, J. Phys. B **38**, S707 (2005).
[9] G. Weber, H. Bräuning, S. Hess, R. Märtin, U. Spillmann, and T. Stöhlker, J. Instrum. **5**, C07010 (2010).
[10] D. H. Bilderback, P. Elleaume, and E. Weckert, J. Phys. B **38**, S773 (2005).
[11] K.-H. Blumenhagen *et al.* (unpublished).
[12] W. Franz, Z. Phys. **98**, 314 (1936).
[13] L. Kissel and R. H. Pratt, in *Atomic Inner-shell Physics*, edited by B. Crasemann (Plenum Press, New York, 1985), pp. 465–498.
[14] G. E. Brown, R. E. Peierls, and J. B. Woodward, Proc. R. Soc. London A **227**, 51 (1954).
[15] S. Brenner, G. E. Brown, and J. B. Woodward, Proc. R. Soc. London A **227**, 59 (1954).
[16] G. E. Brown and D. F. Mayers, Proc. R. Soc. London A **234**, 387 (1956).
[17] G. E. Brown and D. F. Mayers, Proc. R. Soc. London A **242**, 89 (1957).
[18] W. R. Johnson and K.-T. Cheng, Phys. Rev. A **13**, 692 (1976).
[19] L. Kissel, R. H. Pratt, and S. C. Roy, Phys. Rev. A **22**, 1970 (1980).
[20] P. P. Kane, L. Kissel, R. H. Pratt, and S. C. Roy, Phys. Rep. **140**, 75 (1986).
[21] S. C. Roy, B. Sarkar, L. D. Kissel, and R. H. Pratt, Phys. Rev. A **34**, 1178 (1986).
[22] S. C. Roy, L. Kissel, and R. H. Pratt, Rad. Phys. Chem. **56**, 3 (1999).
[23] A. Costescu, K. Karim, M. Moldovan, S. Spanulescu, and C. Stoica, J. Phys. B **44**, 045204 (2011).

[24] L. Safari, P. Amaro, S. Fritzsche, J. P. Santos, S. Tashenov, and F. Fratini, Phys. Rev. A **86**, 043405 (2012).
[25] A. Surzhykov, V. A. Yerokhin, T. Jahrsetz, P. Amaro, Th. Stöhlker, and S. Fritzsche, Phys. Rev. A **88**, 062515 (2013).
[26] A. Surzhykov, V. A. Yerokhin, Th. Stöhlker, and S. Fritzsche, J. Phys. B **48**, 144015 (2015).
[27] L. Safari, P. Amaro, J. P. Santos, and F. Fratini, Rad. Phys. Chem. **106**, 271 (2015).
[28] C.-P. Lin, K.-T. Cheng, and W. R. Johnson, Phys. Rev. A **11**, 1946 (1975).
[29] V. B. Berestetsky, E. M. Lifshitz, and L. P. Pitaevsky, *Quantum Electrodynamics* (Pergamon Press, Oxford, 1982).
[30] V. M. Shabaev, Izv. Vuz. Fiz. **33**, 43 (1990) [Sov. Phys. J. **33**, 660 (1990)].
[31] V. M. Shabaev, Teor. Mat. Fiz. **82**, 83 (1990) [Theor. Math. Phys. **82**, 57 (1990)].
[32] V. M. Shabaev, Phys. Rep. **356**, 119 (2002).
[33] P. Indelicato, V. M. Shabaev, and A. V. Volotka, Phys. Rev. A **69**, 062506 (2004).
[34] A. V. Volotka, A. Surzhykov, V. M. Shabaev, and G. Plunien, Phys. Rev. A **83**, 062508 (2011).
[35] D. A. Varshalovich, A. N. Moskalev, and V. K. Khersonskii, *Quantum Theory of Angular Momentum* (World Scientific, Singapore, 1988).
[36] E. H. Wichmann and N. M. Kroll, Phys. Rev. **101**, 843 (1956).
[37] J. Sapirstein and W. R. Johnson, J. Phys. B **29**, 5213 (1996).
[38] V. M. Shabaev, I. I. Tupitsyn, V. A. Yerokhin, G. Plunien, and G. Soff, Phys. Rev. Lett. **93**, 130405 (2004).
[39] V. A. Yerokhin and V. M. Shabaev, Phys. Rev. A **60**, 800 (1999).
[40] V. A. Yerokhin and A. Surzhykov, Phys. Rev. A **82**, 062702 (2010).
[41] V. A. Yerokhin and A. Surzhykov, Phys. Rev. A **84**, 032703 (2011).
[42] B. Zhou, L. Kissel, and R. H. Pratt, Phys. Rev. A **45**, 2983 (1992).
[43] B. Zhou, L. Kissel, and R. H. Pratt, Phys. Rev. A **45**, 6906 (1992).